Eur. Phys. J. B **16**, 251–259 (2000)

THE EUROPEAN PHYSICAL JOURNAL B

EDP Sciences

Resonant Raman scattering in the superconducting cuprates: Frozen-phonon versus perturbational approach

E.Ya. Sherman[1,2,a] and C. Ambrosch-Draxl[1]

[1] Institute for Theoretical Physics, University Graz, Universitätsplatz 5, 8010, Graz, Austria
[2] Moscow Institute of Physics and Technology, 141700 Dolgoprudny, Moscow Region, Russia

Received 8 December 1999

Abstract. We consider in detail Raman scattering by vibration of the apical oxygen ions in the $RBa_2Cu_3O_7$ superconducting cuprates. The scattering intensity is very sensitive to the ratio of diagonal and off-diagonal matrix elements of electron-phonon coupling, bandstructure, and carrier concentration. Our results show a large quantitative difference between the results of frozen-phonon and perturbational approach to the Raman process. The discrepancy becomes especially large when interband transitions to the states near the Fermi level are close to resonance with the incident light. The calculation of phonon-induced ion charge fluctuations shows an analogous discrepancy. The reason for these effects is the possibility of carrier redistribution between different parts of the Fermi surface arising in the frozen-phonon approximation. Our results show that Raman scattering in superconducting superlattices is very sensitive to the properties of the states near the Fermi level. For this reason experiments performed on the superlattices can help to resolve the discrepancy.

PACS. 63.20.Kr Phonon-electron and phonon-phonon interaction – 74.25.Jb Electronic structure – 74.25.Kc Phonons

1 Introduction

The bandstructure of solids at an energy scale of several eV can be probed by optical spectroscopy. Ellipsometric measurements can give precise values of the real and imaginary part of the dielectric tensor components $\epsilon_{\alpha\beta}(\omega)$ with α and β being Cartesian indices. However, it is often hard to determine the contribution of specific transitions between different electronic bands to $\epsilon_{\alpha\beta}(\omega)$. This problem can be partially solved by light scattering spectroscopy. Light scattering by lattice vibrations provides a possibility to determine the contribution of those electron states which are related to ions vibrating in the considered phonon mode.

The high-T_c superconductors show interesting Raman spectra in the scattering by phonons as well by electronic excitations. Phonon frequencies and damping were investigated by Raman spectroscopy [1]. Important information about electron-phonon coupling, magnitude and symmetry of the superconducting gap was obtained from the phonon self-energy effects when the crystal is cooled below the transition temperature T_c [2]. All these effects are mainly related to the low-energy electronic states near the Fermi level [3,4]. At the same time, Raman spectroscopy offers a possibility to investigate the bandstructure of a crystal on a much larger energy scale. This can be done by studying the resonant behavior of the Raman scattering intensity as a function of the exciting light frequency ω. The local density approximation applied for the calculation of Raman scattering intensity by the A_{1g} modes in $YBa_2Cu_3O_7$ [5–7] extended the understanding of the Raman process in the superconducting cuprates. A considerable mixing of atomic vibrations within the fully symmetrical phonon modes in many high-T_c compounds [5,8–10] strongly influences the scattering intensity.

In the $RBa_2Cu_3O_7$ crystals (where R is a rare-earth atom) the strongest contribution to the phonon Raman scattering comes from the electronic states related to the Cu1-O1-$(O4)_2$ chains. (Being strongly bound to the Cu1-O chains, the apical oxygen is also regarded as a chain atom here.) The strongest mode is the fully symmetrical out-of-phase vibration of the pair of apical oxygen ions. This A_{1g} mode has a frequency of approximately 500 cm^{-1} in all these compounds [1]. In this paper, we investigate light scattering by this vibration and its relation to the electronic bands exhibiting the character of the chain atoms.

The interest to this investigation is motivated at least by the following reasons:

First, a considerable part of the superconducting condensate is related to the chains making them important for the formation of the superconducting state. As it was shown by Combescot and Leyronas [11,12], the coupling

[a] e-mail: eugene.sherman@kfunigraz.ac.at

between chains and planes can be responsible for the symmetry of the order parameter. Vibrations of the apical oxygen naturally modulates the plane-chain coupling [9]. The chains induce an anisotropy of the bandstructure and the superconducting gap and thus lead to the so-called "$d + s$" pairing [13] observed by electronic Raman scattering [14].

Second, the intensity of the apical oxygen mode increases approximately by a factor of two by cooling the crystal below T_c [15,16]. This increase shows a clear dependence on ω and on the polarization direction of the incident and scattered light. The large effect cannot be explained without taking into account that the mechanism of Raman scattering is related to the electronic states in the copper-oxygen chain band.

The third reason is related to the puzzling properties of the $PrBa_2Cu_3O_7$ compound and $(PrBa_2Cu_3O_7)_m(YBa_2Cu_3O_7)_n$ superlattices, where m and n are the number of the Pr- and Y layers per the superlattice unit cell. The Pr-based cuprate does not demonstrate the superconducting transition and is the only exception among the $RBa_2Cu_3O_7$ family. A qualitative analysis of its intriguing behavior was presented by Mazin [17]. Experimental results of Takenaka *et al.* show that the chains in this compound exhibit the same properties as in all others, however, the CuO_2 planes are quite different from their counterparts [18]. The superlattices demonstrate physical properties intermediate between the pure $PrBa_2Cu_3O_7$ and $YBa_2Cu_3O_7$ compounds. The presence of Pr layers decreases the transition temperature and causes a charge transfer between different layers within the elementary cell [19,20]. New intense phonon peaks in the Raman spectra of the superlattices are a consequence of the charge transfer [21]. The $(m : n)$ - ratio can artificially govern the amount of carriers in the chains [19]. As we will see below, the Raman intensity is sensitive to the carrier concentration, and, therefore, it should be possible to extract its value from the Raman data.

There are two different approaches for the calculation of Raman intensities. One of them is the "frozen-phonon approximation" [22], widely used for the investigation of phonon properties of solids. The other method is the application of perturbation theory [23] based on the analysis of Feynman graphs describing the scattering. A big advantage of the first technique is that it is well-adopted for first-principles calculations for the bandstructures of crystals [5–7]. Below we will show with a simple model that being applied to a metal, in particular to a high-T_c compound, these approaches can give quantitatively different results. The discrepancy becomes large in case of resonant Raman scattering when the photon energy is close to energies of interband transitions in the vicinity of the Fermi surface.

The paper is organized as follows: First, we will present the tight binding model of copper-oxygen chains including the apical oxygen, and apply it to the investigation of electron-phonon and electron-light coupling. On this basis we will investigate the perturbational and the frozen-phonon technique for the calculation of Raman intensities, present the results of these two different approaches and compare them for several values of the model parameters. In addition, we will consider the phonon-driven charge redistribution within the chains and between the chains and the CuO_2 planes. These fluctuations and their relation to the Raman scattering will be investigated within both the approaches, that give different results in this case too.

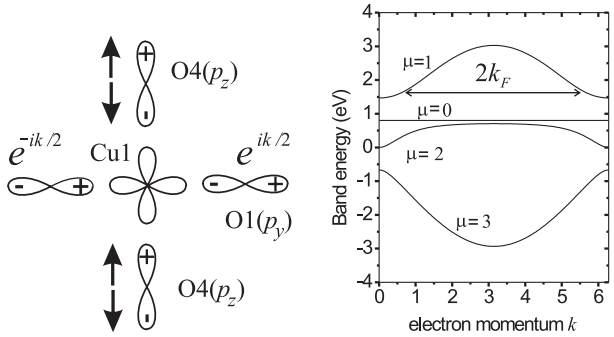

Fig. 1. (a) Orbitals included in the tight-binding model. Arrows show displacement of the O4 ions in the A_{1g} mode. (b) The bandstructure for the parameters adopted in the text.

2 Bandstructure, electron-phonon and electron-light coupling

2.1 Tight-binding model

Raman scattering is a result of indirect interaction of the lattice with light propagating in a solid. This interaction shows up as the influence of the phonon on the dielectric function. In order to calculate the phonon Raman scattering intensity three ingredients are required: (1) bandstructure, (2) electron-light coupling, characterized by matrix elements of the dipole transitions between the bands and (3) electron-phonon coupling matrix elements. To obtain all these components we shall apply the tight-binding model which allows to get reasonable results under simplified conditions [24].

We consider the Cu1-O1-$(O4)_2$ chain element of unit cell consisting of Cu1, chain oxygen O1 and the pair of the apical oxygen O4 atoms, as shown in Figure 1a. The tight-binding wave function is:

$$|\mu, k\rangle \equiv \Psi_{\mu,k} = \frac{1}{\sqrt{N}} \sum_{l,o} \eta_{\mu,o}(k)\, \psi_o(\mathbf{r} - \mathbf{R}_{l,o})\, \mathrm{e}^{\mathrm{i}ky_{l,o}}, \quad (1)$$

where k is the electron momentum along the chain (y axis), $\mathbf{R}_{l,o}$ are the lattice site vectors with the index o enumerating the orbital wave functions $\psi_o(\mathbf{r} - \mathbf{R}_{l,o})$. Here, $o = 1$ corresponds to the Cu1($d_{z^2-y^2}$) orbital, $o = 2$ describes O1(p_y) states, and $o = 3, 4$ refer to the pair of O4(p_z), respectively. The index μ marks the bands, $\eta_{\mu,o}(k)$ are the tight-binding coefficients, and N is the number of unit cells. We suppose that the lattice constant along the chain is equal to unity, and the $y-$coordinates

of the O1 ions are $n + 1/2$, where n is an integer. The model Hamiltonian is written as:

$$\hat{H} = \begin{bmatrix} 0 & \mathrm{i}st_\mathrm{c} & t_\mathrm{a} & -t_\mathrm{a} \\ -\mathrm{i}st_\mathrm{c} & E_\mathrm{c} & 0 & 0 \\ t_\mathrm{a} & 0 & E_\mathrm{a} & 0 \\ -t_\mathrm{a} & 0 & 0 & E_\mathrm{a} \end{bmatrix}, \qquad (2)$$

where $s = 2\sin(k/2)$. The Hamiltonian includes the Cu1-O4 hopping element t_a, Cu1-O1 hopping t_c, and the energy differences E_c and E_a of the oxygen orbitals in the chain and the apical site, respectively, with respect to the Cu1 site energy assumed to be zero. For the Hamiltonian in equation (2) we find four electron bands, depicted in Figure 1b. Three of them have finite dispersion and wave functions even with respect to the reflection in the (xy) plane. The fourth band with the energy $E_0(k) = E_\mathrm{a}$ is flat, its wave function is odd with respect to the reflection and purely consists of the two O4 orbitals decoupled from Cu1 and O1. The Fermi level intersects the upper band $E_1(k)$ such that the Fermi energy $E_\mathrm{F} = E_1(k_\mathrm{F})$, and the Fermi momentum k_F is counted from the π-point. We accept the band structure parameters $E_\mathrm{c} = 0$, E_a=0.8 eV, $t_\mathrm{c} = 1.4$ eV, $t_\mathrm{a} = 0.7$ eV, and $k_\mathrm{F} = 0.8\pi$ to get an agreement with the first-principles bandstructure [6,7].

2.2 Electron-phonon and electron-light coupling

When the ions are displaced from their equilibrium positions, the electron site energies and intersite hopping matrix elements are perturbed. Therefore, a perturbation should be added to the tight-binding Hamiltonian in equation (2). For the out-of-phase vibration of the apical oxygen ions along the z-axis, the perturbation includes diagonal and non-diagonal matrix elements of electron-phonon coupling:

$$\hat{H}_\mathrm{e-ph} = \mathcal{Q} \begin{bmatrix} 0 & 0 & C_\mathrm{t} & -C_\mathrm{t} \\ 0 & 0 & 0 & 0 \\ C_\mathrm{t} & 0 & C_\mathrm{E} & 0 \\ -C_\mathrm{t} & 0 & 0 & C_\mathrm{E} \end{bmatrix}, \qquad (3)$$

where $\mathcal{Q}$ is the O4 ion displacement, while C_E and C_t are deformation potentials, corresponding to the changes in the site energy and hopping, respectively. Note that $C_\mathrm{t} \leq 0$ since the hopping is diminished with increasing Cu1-O4 distance. The interplay of C_E and C_t will result in an effective k-dependent deformation potential, that determines the shift of the band energies. For a given field $V(\mathbf{r})$ within the unit cell, the deformational potentials can be calculated as

$$\begin{aligned} C_\mathrm{E} &= \int \psi_4^2 \left(\mathbf{r} - \mathbf{R}_{l,3}\right) \nabla V(\mathbf{r}) \mathrm{d}^3 r, \\ C_\mathrm{t} &= \int \psi_4 \left(\mathbf{r} - \mathbf{R}_{l,4}\right) \psi_1 \left(\mathbf{r} - \mathbf{R}_{l,1}\right) \nabla V(\mathbf{r}) \mathrm{d}^3 r \\ &\quad + \int \psi_4 \left(\mathbf{r} - \mathbf{R}_{l,4}\right) V(\mathbf{r}) \nabla \psi_1 \left(\mathbf{r} - \mathbf{R}_{l,1}\right) \mathrm{d}^3 r. \end{aligned} \qquad (4)$$

The potential C_E arises due to the asymmetric crystalline environment of the O4 site located between the Cu-O1 chain and the CuO_2 plane. The asymmetry is mainly determined by Coulomb forces due to the high charge density in the planes, that is approximately two electrons per CuO_2 formula. The second contribution, C_t, is nonzero even for a crystal field which is symmetric with respect to reflection in the horizontal plane containing the O4 ions. Mapping the tight-binding model onto the first-principle results [6,7] yields $C_\mathrm{E} \approx 10$ eV/Å, and $C_\mathrm{t} \approx -5$ eV/Å.

Proceeding now to a momentum representation, we rewrite our Hamiltonian for zero-momentum Raman-active phonons in the following form:

$$\widehat{H}_\mathrm{e-p} = \frac{z_0}{\sqrt{2N}} \sum_{\mu,\mu'} \sum_k g_{\mu,\nu}(k) \left(\hat{a}^+ + \hat{a}\right) \widehat{c}^+_{\mu,k} \widehat{c}_{\nu,k}. \qquad (5)$$

Here $z_0 = \sqrt{\hbar/2M\Omega}$ denotes the zero-point vibrational amplitude, M is the oxygen mass, and Ω is the phonon frequency (we put $\hbar = 1$ below), $\hat{a}^+(\hat{a})$ is the phonon creation (annihilation) operator, while $\widehat{c}^+_{\mu,k}$ $(\widehat{c}_{\nu,k})$ is the corresponding operator for electrons. The interband and intraband matrix elements in equation (5) can be obtained by

$$g_{\mu,\nu}(k) = \sum_{o_1,o_2} \eta^*_{\mu,o_1}(k) \left(\hat{H}_\mathrm{e-ph} \mathcal{Q}^{-1}\right) \eta_{\nu,o_2}(k). \qquad (6)$$

To describe coupling to light, we use the dipole approximation, where the interaction of an electron with the electric field $\mathbf{E}$ is given by $\widehat{V}_\mathrm{e-l} = -e\mathbf{E}\mathbf{r}$, where e is the electron charge (we assume $e = -1$ below). The interband matrix elements of the radius-vector components between the $|\nu, k\rangle$ and $|\mu, k\rangle$ band states are:

$$\begin{aligned} \langle \mu k | \widehat{z} | \nu k \rangle &= \mathcal{R}_z \sum_{o_1,o_2} \eta^*_{\mu,o_1}(k) \, \Pi^z_{o_1,o_2} \eta_{\nu,o_2}(k), \\ \langle \mu k | \widehat{y} | \nu k \rangle &= \mathcal{R}_y \cos(k/2) \sum_{o_1,o_2} \eta^*_{\mu,o_1}(k) \Pi^y_{o_1,o_2} \eta_{\nu,o_2}(k) \end{aligned} \qquad (7)$$

where the matrices $\Pi^\alpha_{o_1,o_2}$ have the following form:

$$\Pi^z_{o_1,o_2} = \begin{bmatrix} 0&0&1&1 \\ 0&0&0&0 \\ 1&0&0&0 \\ 1&0&0&0 \end{bmatrix}, \qquad \Pi^y_{o_1,o_2} = \begin{bmatrix} 0&1&0&0 \\ 1&0&0&0 \\ 0&0&0&0 \\ 0&0&0&0 \end{bmatrix}. \qquad (8)$$

Here $\mathcal{R}_\alpha$ is the matrix element of the radius-vector component $\hat{r}_\alpha$ between Cu2$(d_{z^2-y^2})$ and O(p_α) states within the unit cell. Non-zero nondiagonal components in $\Pi^z_{o_1,o_2}$ and $\Pi^y_{o_1,o_2}$ correspond to Cu1-O4 and Cu1-O1 transitions, respectively. The factor $\cos(k/2)$ in equation (7) appears due to the Bloch exponents $\exp(-\mathrm{i}k/2)$ and $\exp(\mathrm{i}k/2)$ related the O1 ions from the nearest-neighbor unit cells, as shown in Figure 1a. At the Brillouin zone boundary $k = \pm\pi$ the matrix element of $\widehat{y}$ vanishes due to symmetry. On these planes, the oxygen orbitals O1(p_y) surrounding the Cu1 ion form even state with respect to the $y \longleftrightarrow -y$ reflection. The $d_{z^2-y^2}$ orbital is also even, thus the corresponding matrix element of the odd $\widehat{y}$ operator is zero.

3 Raman scattering

3.1 Frozen-phonon approach

In order to investigate the Raman scattering, let us consider a light beam propagating in a solid characterized by a dielectric tensor $\epsilon_{\alpha\beta}(\omega) = 1 + 4\pi\chi_{\alpha\beta}(\omega)$ with $\chi_{\alpha\beta}(\omega)$ being the polarizability. The nonzero components of the contribution of the Cu-O1-$(O4)_4$ chains to the polarizability for the model chosen above are given by:

$$\chi_{\alpha\alpha}(\omega) = 2\int_{-k_{\rm F}}^{k_{\rm F}} \chi_{\alpha\alpha}(\omega,k)\frac{{\rm d}k}{2\pi},$$
$$\chi_{\alpha\alpha}(\omega,k) = \sum_{i,f}\left|\langle fk|\,\hat{M}_\alpha\,|ik\rangle\right|^2\left[\frac{1}{\omega_{fi}(k)-\omega-{\rm i}\Gamma} + \frac{1}{\omega_{fi}(k)+\omega-{\rm i}\Gamma}\right]. \quad (9)$$

Here $\langle fk|\,\hat{M}_\alpha\,|ik\rangle$ is the dipole matrix element ($\hat{M}_\alpha = -r_\alpha$) between the initial (occupied) and final (empty) band states, $\omega_{fi}(k) = E_f(k) - E_i(k)$, 2 is the spin factor, and $k_{\rm F}$ is the Fermi momentum. Γ is the lifetime broadening of the final state $|fk\rangle$, which we will assume Γ =0.1 eV below. For $\chi_{zz}(\omega)$ only initial flat band gives a nonzero dipole matrix element, while for $\chi_{yy}(\omega)$ the two dispersive bands below the Fermi level contribute to the polarizability.

To understand how lattice vibrations scatter the light, we start with the frozen-phonon approximation developed for Raman scattering by Mills, Maradudin, and Burstein [22]. Within this approach, the phonon is considered as an infinitely slow ionic displacement, that at each time t leads to a static perturbation within the unit cell as written in equation (3). For the band state $|\mu k\rangle$ this perturbation shifts the energy and makes the wave function dependent on the ion displacements. For these reasons the lattice vibration causes a modulation of the dielectric function, and we obtain for the phonon-induced variation:

$$\delta\chi_{\alpha\alpha}(\omega) = 2\mathcal{Q}\frac{\partial}{\partial\mathcal{Q}}\chi_{\alpha\alpha}(\omega), \quad (10)$$

where the factor 2 appears since two ions vibrate in the mode. As a result, a peak is observed in the light scattering spectrum at the frequency Ω. The full Raman intensity integrated over the phonon peak is given by

$$I_{\alpha\alpha}(\omega) \sim \omega^4\delta_{l,\alpha}\left\langle\mathcal{Q}^2\right\rangle\left|{\rm d}\chi_{\alpha\alpha}(\omega)/{\rm d}\mathcal{Q}\right|^2, \quad (11)$$

where $\delta_{l,\alpha}$ is the light penetration depth for the given light polarization. Here we have assumed that the incident and scattered light are polarized along the α-direction.

As we can conclude from equation (9), the change in the polarizability due to displacement of ions can be represented by the sum of four terms:

$$\delta\chi_{\alpha\alpha} = \delta\chi^E_{\alpha\alpha} + \delta\chi^\eta_{\alpha\alpha} + \delta\chi^{\mathcal{R}_\alpha}_{\alpha\alpha} + \delta\chi^{k_{\rm F}}_{\alpha\alpha}. \quad (12)$$

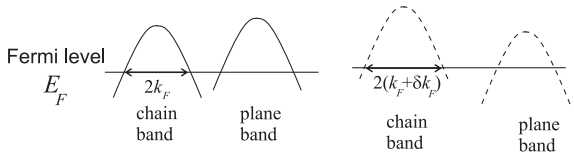

Fig. 2. Charge redistribution between the plane and chain bands. The solid lines correspond to the unperturbed bands, while the dashed lines show the phonon-driven changes in the band energies, and, in turn, in the carrier redistribution.

The first term arises due to changes in the band energies, which have the form $\delta E_\mu(k) = \mathcal{Q}g_{\mu\mu}(k)$, and, in turn, $\delta\omega_{fi} = [g_{ff}(k) - g_{ii}(k)]\,\mathcal{Q}$. Since the band energies and the interband distances are variated by the perturbation, the polarizability is changed as well, as we can see in equation (9). The second contribution is due to changes in the electronic wave function. The variation of the tight-binding coefficients included in the matrix elements of $\hat{M}_\alpha$ is given by perturbation theory as:

$$\delta\eta_{\mu,o}(k) = \mathcal{Q}\sum\frac{g_{\nu\mu}(k)}{E_\mu(k) - E_\nu(k)}\eta_{\nu,o}(k). \quad (13)$$

The origin of the third term, $\delta\chi^{\mathcal{R}_\alpha}_{\alpha\alpha}$, is related to the fact that the overlap of the Cu1 and O4 orbitals strongly depends on the Cu1-O4 distance and therefore is modulated by the phonon. Since $\delta\omega_{fi}(k)$ leads to a variation of the denominator in the second line of equation (9), $\delta\chi^E_{\alpha\alpha}$ corresponds to a strong dependence of the scattering intensity on the light frequency, whereas the change of the matrix causes a weaker one.

The last contribution, $\delta\chi^{k_{\rm F}}_{\alpha\alpha}$, has a collective many-particle origin specific for metals. It arises from a change of the Fermi surface driven by the ion displacements. For the case of our interest it is due to the following effect: In $RBa_2Cu_3O_7$ the copper-oxygen chains are in equilibrium with the CuO_2 planes having the common Fermi energy $E_{\rm F}$. For the problem considered the planes play a role of a charge reservoir. The O4 vibration influences mainly the states in the chains, leading to a charge redistribution between the chain and plane bands in order to keep their Fermi energies equal and the total amount of carriers constant (see Fig. 2). This variation of the concentration and, in turn $k_{\rm F}$, can be easily calculated as

$$\delta k_{\rm F} = -\pi\delta E(k_{\rm F})\frac{N_{\rm c}N_{\rm p}}{N_{\rm c}+N_{\rm p}}, \quad (14)$$

where $N_{\rm c}$ and $N_{\rm p}$ are the density of states at the Fermi level for the chain band, and both the plane bands, respectively. $\delta E(k_{\rm F})$ in equation (14) is the shift of the energy for the $\pm k_{\rm F}$ states determined by intraband electron-phonon coupling which is $\delta E(k_{\rm F}) = \mathcal{Q}g_{11}(k_{\rm F})$. The electron redistribution leads to the $\delta\chi^{k_{\rm F}}_{\alpha\alpha}$ term in equation (10). The shift of the Fermi level due to change of the concentration of the carriers within the chains is given by:

$$\delta E_{\rm F} = \delta E(k_{\rm F}) + \frac{1}{\pi}\frac{\delta k_{\rm F}}{N_{\rm c}} = \delta E(k_{\rm F})\frac{N_{\rm c}}{N_{\rm c}+N_{\rm p}}\,. \quad (15)$$

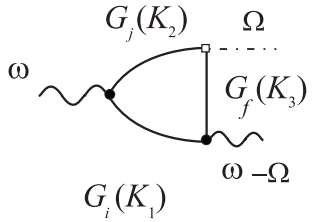

Fig. 3. Feynman graph for Raman scattering. The solid lines describe electrons, the wavy lines correspond to photons while dashed-dot line presents the phonon. Black circles present the interband matrix elements of the dipole momentum while the white square is the matrix element of electron-phonon coupling.

Since the Fermi surface in the planes is close to a Van Hove singularity, one can expect $N_\mathrm{p} \gg N_\mathrm{c}$, resulting in a pinning of the Fermi level with $\delta E_\mathrm{F} \ll \delta E(k_\mathrm{F})$ [25].

3.2 Perturbational approach and Feynman graphs

Another approach to the calculation of the Raman intensity is based on perturbation theory. There the scattering occurs due to a virtual excitation of an electron-hole pair by incident light. Due to electron-phonon coupling a component of the pair (electron or hole) excites a phonon and the pair recombines emitting a scattered photon. This process is described by the Feynman graph shown in Figure 3. To get the total matrix element of the transition between initial and final state we sum up the graphs corresponding to all possible processes, which include alternative ordering of the electron-phonon and electron-light coupling matrix elements and bands. The corresponding expression for effective phonon-light coupling matrix element $\gamma_{\alpha\alpha}(k,\omega)$ at a given k has the form

$$\gamma_{\alpha\alpha}(k,\omega) = \sum_{i,j,f} \gamma_{\alpha\alpha}(k,\omega|j,f,i),$$

$$\gamma_{\alpha\alpha}(k,\omega|j,f,i) = \int \langle ik|\,\hat{r}_\alpha\,|jk\rangle\, G_j(K_3) g_{jf}(k) G_f(K_2) \times \langle fk|\,\hat{r}_\alpha\,|ik\rangle\, G_i(K_1) \frac{\mathrm{d}E}{2\pi}, \quad (16)$$

where we again assume the incident and scattered light to be polarized along the α-direction. The 4-vectors are determined as $K_1 = (E,k)$, $K_2 = (E+\omega,k)$, $K_3 = (E+\omega-\Omega,k)$ and the Green's functions are defined as:

$$G_\mu(E,k) = \frac{1}{E - E_\mu(k) + \mathrm{i}\Gamma_\mu \mathrm{sign}\,[E_\mu(k) - E_\mathrm{F}]}, \quad (17)$$

where $\Gamma_1 = \Gamma$ and $\Gamma_{\mu\neq 1} = 0$. After integration over the momentum we find the Raman matrix element

$$\mathrm{R}_{\alpha\alpha}(\omega) = \int_{-k_\mathrm{F}}^{k_\mathrm{F}} \gamma_{\alpha\alpha}(k,\omega) \frac{\mathrm{d}k}{2\pi}, \quad (18)$$

and the Raman intensity

$$I_{\alpha\alpha}(\omega) \sim \delta_{l,\alpha} \left|\mathrm{R}_{\alpha\alpha}(\omega)\right|^2. \quad (19)$$

There are two different kinds of Feynman graphs for the phonon Raman scattering. The first one describes a phonon coupling electron bands with the same occupancy ($n_j = n_f = 0$ or $n_j = n_f = 1$), whereas the other graphs involve a phonon coupling one empty and one occupied band state ($n_j \neq n_f$). For the two processes, integration over energy E in equation (16) yields a (k,ω)-dependence of the matrix element:

$$\gamma_{\alpha\alpha}(k,\omega|j,f,i) \sim \frac{\langle ik|\,\hat{r}_\alpha\,|jk\rangle\, g_{jf}(k)\, \langle fk|\,\hat{r}_\alpha\,|ik\rangle}{\omega - \omega_{fi}(k)} \times \begin{cases} \dfrac{1}{\omega - \omega_{ji}(k)}, & n_j = n_f \\ \dfrac{1}{\omega_{fj}(k)}, & n_j \neq n_f. \end{cases} \quad (20)$$

From equations (9, 12), and (20) we find a correspondence between the frozen-phonon and perturbative approaches. The sum of the Feynman graphs, where a phonon couples the same electron states ($f = j$), corresponds to the term determined by $\delta\omega_{fi}(k)$ in the frozen-phonon approximation. It can be readily seen from the same resonance dependence of the processes, namely $\partial\chi_{\alpha\alpha}(\omega,k)/\partial\omega_{fi}(k) \sim [\omega - \omega_{fi}(k)]^{-2}$, demonstrating the same behavior as $\gamma_{\alpha\alpha}(k,\omega|j,f,i)$ for $j = f$. The $n_j \neq n_f$ graph being less resonant leads to the Raman intensity arising due to a phonon-driven polarization of wave functions, that is to $\partial\eta_{\mu,o}(k)/\partial\mathcal{Q}$. This derivative being obtained from equation (13) is proportional to $\omega_{fj}^{-1}(k)$, like the contribution of the $n_j \neq n_f$ graph in equation (20).

3.3 Charges of ions

Since the atomic displacements induce changes in the site energies and hopping matrix elements, they can cause a charge transfer between the ions in metals [26]. We can calculate now the charge transfer among the chain ions and from the chains to the CuO_2 planes induced by apical oxygen displacement. The charge transfer should minimize the total energy of the system and keep the Fermi energy the same at all the parts of the Fermi surface. The first process conserves the total charge of the Cu1-O1-$(O4)_2$ complex. The second one changes it so that the Fermi energy remains equal for the chains and planes.

The mobile carriers in $RBa_2Cu_3O_7$ correspond to the hole band states above the Fermi level, and, therefore, the charges of the oxygen ions, in which we will be mainly interested, are given by:

$$Q_o = 2 \int_{-k_\mathrm{F}}^{k_\mathrm{F}} \left|\eta_{1,o}(k)\right|^2 \frac{\mathrm{d}k}{2\pi}, \quad (21)$$

where 2 is the spin factor. Note that Q_o in equation (21) is positive since we supposed that O^{2-} ions have zero charge.

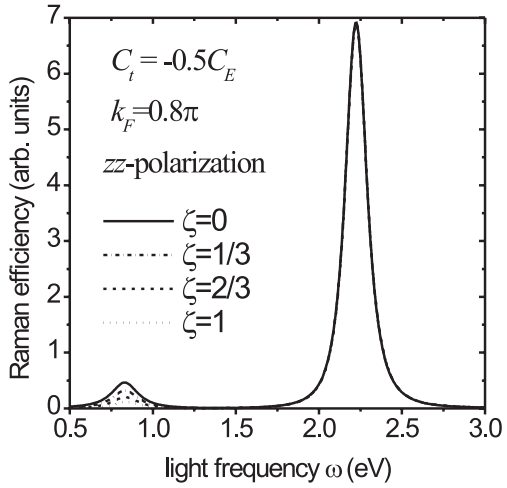

Fig. 4. Raman efficiency calculated in the frozen-phonon approximation in zz-polarization for different values of ζ, with $C_{\rm t} = -0.5C_{\rm E}$. For the strong peak at $\omega \approx 2.3$ eV related to transition to the top of the $\mu = 1$ band, the result is ζ-independent.

Since the charges are determined by the coefficients of the tight-binding wave function and integration over the states with $-k_{\rm F} < k < k_{\rm F}$, their changes consist of two terms, analogously to the contributions to the Raman matrix element:

$$\delta Q_o = \delta Q_o^{\eta} + \delta Q_o^{k_{\rm F}}. \tag{22}$$

Here, δQ_o^{η} arises due to a modulation of the tight-binding wave functions. The second term, $\delta Q_o^{k_{\rm F}}$, is determined by the variation in the Fermi momentum, arising from a possible charge transfer between the Cu-O1-$(O4)_2$ chains and CuO_2 planes, that is analogous to equation (14). The perturbational approach gives only the first contribution calculated as

$$\delta Q_o^{\eta} = 4 \int_{-k_{\rm F}}^{k_{\rm F}} \eta_{1,o}(k) \delta\eta_{1,o}(k) \frac{{\rm d}k}{2\pi}, \tag{23}$$

where we supposed that $\eta_{1,o}(k)$ is real. Changes in the wave functions $\delta\eta_{1,o}(k)$ shown in equation (13) are due to interband matrix elements of the electron-phonon coupling. The second term is given by

$$\delta Q_o^{k_{\rm F}} = 4\eta_{1,o}^2(k_{\rm F})\,\delta k_{\rm F}, \tag{24}$$

where $\delta k_{\rm F}$ is determined by equation (14).

4 Results and discussion

4.1 Raman efficiency

Figure 4 presents the calculated Raman efficiency $\left|\mathcal{R}_z^{-1}\partial\chi_{zz}(\omega)/\partial\mathcal{Q}\right|^2$ obtained within the frozen-phonon approach for different $\zeta = N_{\rm p}/(N_{\rm p}+N_{\rm c})$ values. The solid line corresponds to $\zeta = 0$, and, therefore, describes also the perturbational result, where no charge redistribution between the planes and chains is possible. The first peak at approximately 0.7 eV corresponds to the transition from the $\mu = 0$ band to the Fermi level while the second one at $\omega \approx 2.3$ eV comes from the transition to the top of the band ($k = \pi$). The intensity of the latter is enhanced by the infinite density of states (Van Hove singularity) near the band top. We should note, however, that the resonance frequency of the first peak is too low for experimental observation. The situation is quite different for the yy-polarization. It does not demonstrate resonance due to transition to the top of the upper band, since according to equation (7), the interband matrix element at $k = \pi$ is zero. The two peaks shown in Figure 5a arise due to transitions to the Fermi level from the bands 2 and 3, respectively.

The interplay of the parameters $C_{\rm E}$ and $C_{\rm t}$ doesn't change the peak positions but crucially influences the ratio of the peak intensities and shape of the resonance curve in the yy-polarization, as we can clearly see from comparison of Figures 5a and b, that present the Raman efficiency for $C_{\rm t}/C_{\rm E} = -0.5$ and $C_{\rm t} = 0$, respectively. Our results qualitatively reproduce the main experimental observations of resonant Raman scattering by the apical oxygen vibration: (i) For $\omega \approx 2.5$ eV the mode shows a sharp resonance in the zz-polarization and a moderate resonance in the yy-polarization. (ii) Raman intensity $I_{zz}(\omega) \gg I_{yy}(\omega)$ in the experimentally investigated region of ω. A direct comparison to the experiment, however, cannot be done at present since the parameters $\mathcal{R}_z$ and $\mathcal{R}_y$ as well as the light penetration depths $\delta_{l,\alpha}$ are not determined within our model. Since the ratio $I_{zz}(\omega)/I_{yy}(\omega)$ is proportional to $(\mathcal{R}_z/\mathcal{R}_y)^4$, detailed information about these parameters is desirable to allow for a quantitative comparison with experimental results.

Regarding the transition to the Fermi level, the frozen-phonon approach can give the scattering intensity considerably different from that for the perturbational one as we can see in Figures 4 and 5. This fact emphasizes the importance of the term $\delta\chi_{\alpha\alpha}^{k_{\rm F}}$. The role of the $\delta k_{\rm F}$ induced contribution can be seen from the following argument. Suppose that the resonance occurs near the Fermi level, that is $\omega = \omega_{fi}(k_{\rm F}) + \Delta$, and $|\Delta| \ll \omega$. Due to the phonon driven changes in the Fermi momentum, according to equation (9) we get for the real and imaginary part of the susceptibility change:

$$\begin{aligned}
{\rm Re}\,\delta\chi_{\alpha\alpha}^{k_{\rm F}} &\sim \delta k_{\rm F} \frac{\Delta}{\Delta^2+\Gamma^2} \left|\langle f k_{\rm F}|\,\hat{M}_\alpha\,|i k_{\rm F}\rangle\right|^2, \\
{\rm Im}\,\delta\chi_{\alpha\alpha}^{k_{\rm F}} &\sim \delta k_{\rm F} \frac{\Gamma}{\Delta^2+\Gamma^2} \left|\langle f k_{\rm F}|\,\hat{M}_\alpha\,|i k_{\rm F}\rangle\right|^2,
\end{aligned} \tag{25}$$

where $\delta k_{\rm F}$ is estimated from equation (14) for $N_{\rm c} \sim N_{\rm p}$ and $N_{\rm c} \sim 1/v_{\rm F}$ ($v_{\rm F}$ is the Fermi velocity) as $\delta k_{\rm F} \sim g_{11}(0)\mathcal{Q}/v_{\rm F} \sim C_{\rm E}\mathcal{Q}/v_{\rm F}$. The effect of the changes in the Fermi momentum is important when Δ approaches zero. At the same time, due to changes in the denominator in equation (9), $\delta\chi_{\alpha\alpha}^{\rm E}$ is of the same order of magnitude as ${\rm Im}\,\delta\chi_{\alpha\alpha}^{k_{\rm F}}$, as we can see when taking the derivative with respect to ω_{fi} in the second line of equation (9).

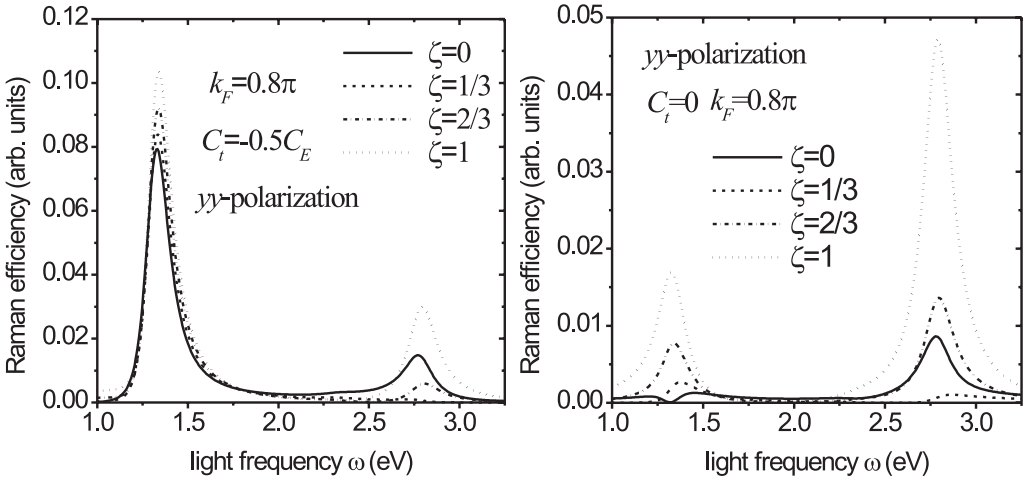

Fig. 5. (a) Raman efficiency as a function of ω in yy-polarization for different values of ζ at $C_{\rm t} = -0.5C_{\rm E}$. The units are same as in Figure 4. (b) Same as Figure 5a, but for at $C_{\rm t} = 0$.

This fact implies that both contributions originating from $\delta k_{\rm F}$ and $\delta\omega_{fi}$, are equally important. Note that for both cases the main contribution to $\delta\chi_{\alpha\alpha}$ comes from changes in the imaginary part of the polarizability. It can be readily understood since in the limit of small Γ, $\mathrm{Im}\,\chi_{\alpha\alpha}$ appears as a step function when a resonance occurs at the Fermi level such that Δ is close to zero.

The contribution of $\delta k_{\rm F}$ requires an infinitely slow perturbation, that keeps the two many-particle system (planes and chains) in equilibrium. Note that a redistribution of electrons occurs between the states with different momenta under a zero-momentum phonon perturbation. To treat such collective effects it is necessary to include relaxation processes in the model, providing the possibility for an electron redistribution between different bands in order to follow the phonon field [27]. For this reason, the process should take into account both, the interband and the in-plane momentum relaxation rate. One-particle effects (changes in energies and wave functions) and collective effects occur at different time scales. The change of electron energy and wave function happens on a short-time scale which is of the order of $E_{\rm F}^{-1}$ where $E_{\rm F} \sim 1$ eV is a characteristic electron band width. Since $E_{\rm F} \gg \Omega$, the frozen-phonon approximation is always valid for $\delta\chi^{E}_{\alpha\alpha}$ and $\delta\chi^{\eta}_{\alpha\alpha}$ terms. In contrast, the redistribution requires the time of interband relaxation and relaxation along the Fermi surface due to impurities, electron-electron correlations, and phonons. The latter might be much larger than $E_{\rm F}^{-1}$ and even than Ω^{-1}. This problem does not arise within the frozen-phonon approximation where the perturbation is infinitely slow. Therefore the perturbative approach could be the more reliable tool of calculation. It is worth noting that the results obtained within density functional theory using the frozen-phonon approximation give the correct value of intensity for the resonance at the top of the band but a higher value for lower frequencies [5]. We suppose that it is partially due to the above mentioned redistribution of charges occurring in the frozen-phonon technique applied there.

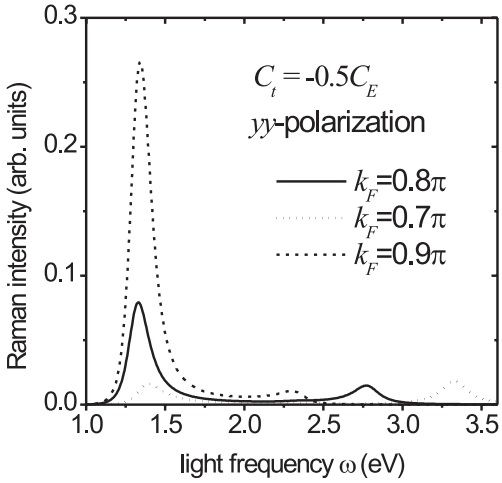

Fig. 6. Raman efficiency in yy-polarization for different values of Fermi momenta for $\zeta = 0$, $C_{\rm t} = -0.5C_{\rm E}$. The units are same as in Figure 4.

Figure 6 presents the resonance behavior obtained with the perturbative approach for the yy-polarization for different Fermi momenta $k_{\rm F}$, and therefore, different hole concentrations within the Cu1-O1-$(O4)_2$ chains. As we discussed in the Introduction, the changes in $k_{\rm F}$ can be achieved in superconducting superlattices. The $k_{\rm F}$-dependence of the Raman spectra is very strong due to changes in the interband distances and effective deformation potentials. The main contribution for the lower-frequency peak, however, is due to the rapid increase in the density of electronic states $N_{\rm c}$ when $k_{\rm F}$ is close to π since the bands $\mu = 2$ and $\mu = 1$ are almost parallel at small k. Their almost parallel dispersions shown in Figure 1b make these bands close to resonance with the incident light in a large part of the Brillouin zone and, therefore, increase the Raman intensity. The dependencies shown in Figure 6 imply that resonant Raman spectra of the $(PrBa_2Cu_3O_7)_m(YBa_2Cu_3O_7)_n$ superlattices

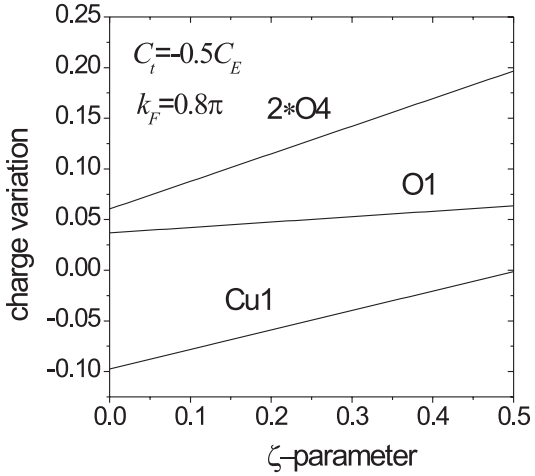

Fig. 7. Phonon-driven charge variations as function of ζ at $C_{\rm t} = -0.5C_{\rm E}$.

in yy-polarization might be strongly sensitive to the $(m : n)$ ratio that governs the carrier concentration in the chains of the Pr- and Y-based subcells. Since adding and depletion of the carriers mainly influences the states near the Fermi surface, comparison of results of experiments performed on different superlattices can help to distinguish between the perturbational and frozen-phonon approach. At the same time, the Raman scattering in zz-polarization in the experimentally achievable region of ω is not considerably influenced by the charge transfer. Unfortunately, to the best of our knowledge, the experimental results are not available at present.

We should briefly mention the role of the term $\delta\chi_{\alpha\alpha}^{\mathcal{R}_\alpha}$ which is related to changes in the overlap of the orbitals. It is not possible to calculate this contribution within our model. However, since it corresponds to non-resonant scattering, it gives only a minor contribution to the intensity. Moreover, it is nonzero only for the zz-polarization. For these reasons we have omitted it in our considerations.

4.2 Charge variations

In Figure 7 we present the derivatives of the ionic charges with respect to the changes in the site energies $\mathrm{d}Q_{\rm o}/\mathrm{d}C_{\rm E}\mathcal{Q}$ for $C_{\rm t} = -0.5C_{\rm E}$ as a function of ζ calculated in the frozen-phonon approximation. The values at $\zeta = 0$ again correspond to the perturbative approach determined by equations (13) and (23). Since $\mathcal{Q}\mathrm{d}Q_{\rm o}/\mathrm{d}C_{\rm E} > 0$ for the oxygen orbitals and $\mathcal{Q}\mathrm{d}Q_{\rm o}/\mathrm{d}C_{\rm E} < 0$ for copper, we conclude that for these parameters some electronic charge goes from the oxygen to the copper sites for positive $\mathcal{Q}$ and *vice versa*. The absolute value $\mathcal{Q}\mathrm{d}Q_{\rm o}/\mathrm{d}C_{\rm E} \sim 10^{-2}$ strongly depends on the contribution of the plane atoms to the density of states. Assuming the ion displacement $\mathcal{Q}$ to be equal to the zero-point vibrational amplitude (≈ 0.05 Å), and $C_{\rm E} = 10$ eV/Å, the phonon-driven apical oxygen charge variation is $\delta Q_4 \sim 10^{-2}$. The positive slope of all the lines in Figure 7 corresponds to the total positive charge coming from the CuO_2 planes to the chains. The $\mathcal{Q}\mathrm{d}Q_2/\mathrm{d}C_{\rm E}$ dependence on ζ is rather weak reflecting the fact that the states near the Fermi level mainly have Cu1 and O4 character. Here we again see a large difference between the frozen-phonon and perturbational approach.

5 Conclusions

The calculation of Raman scattering intensities and phonon-induced charge fluctuations in the superconducting cuprates exhibit a large difference between the frozen-phonon and perturbational approach. Being applied to Raman scattering, these techniques give quantitatively different results in the case of resonant Raman scattering, especially when transitions to the Fermi level are close to resonance with the incident light. A strong effect occurs within the frozen-phonon approach due to a change in the Fermi momentum accompanied by a charge redistribution between the Cu-O1-$(O4)_2$ chains and CuO_2 planes. This effect is absent within the perturbational approach. Analyzing the assumptions made to justify the frozen-phonon approximation, we conclude that perturbation theory could provide the more reliable tool for this kind of calculation. The phonon-driven charge fluctuations being of the order of magnitude of about 10^{-2} are considerably determined by the charge redistribution between the chains and planes too.

Our consideration include the diagonal and non-diagonal electron-phonon coupling. The results show that the Raman intensity is very sensitive to the bandstructure, the carrier concentration and the ratio of electron-phonon coupling parameters. These dependencies imply that these parameters might be extracted from resonant Raman scattering experiments. From this point of view, investigations of resonant Raman scattering in different $(PrBa_2Cu_3O_7)_m(YBa_2Cu_3O_7)_n$ superlattices would be especially interesting since their carrier concentration can be artificially governed by changes in the composition.

We are grateful to the Austrian Science Foundation for support of the projects M534-TPH, P11893-PHY, and P13430-PHY.

References

1. R. Feile, Physica C **159**, 1 (1989).
2. A. Bock, Ann. Physik (Leipzig) **8**, 441 (1999) and references therein.
3. R. Zeyher, G. Zwicknagl, Z. Phys. B **78**, 175 (1990).
4. T.P. Devereaux, Phys. Rev. B **50**, 10287 (1994).
5. E.T. Heyen, S.N. Rashkeev, I.I. Mazin, O.K. Andersen, R. Liu, M. Cardona, J. Jepsen, Phys. Rev. Lett. **65**, 3048 (1990).

6. C. Ambrosch-Draxl, R. Abt, P. Knoll, in *Anharmonic Properties of High -T_c Cuprates*, edited by D. Mihailovic, G. Ruani, E. Kaldis, K.A. Müller (World Scientific, Singapore, 1994), p. 212.
7. C. Ambrosch-Draxl, R. Kouba, P. Knoll, Z. Phys. B **104**, 687 (1997).
8. E.I. Rashba, E.Ya. Sherman, Sov. Phys. JETP Lett. **47**, 482 (1988).
9. E.I. Rashba, E.Ya. Sherman, Superconductivity: Physics, Chemistry, Technique **2**, 80 (1989).
10. O. V. Misochko, E. I. Rashba, E. Ya. Sherman, V.B. Timofeev, Phys. Rep. **194**, 393 (1990).
11. R. Combescot, X. Leyronas, Phys. Rev. Lett. **75**, 3732 (1995).
12. R. Combescot, X. Leyronas, Phys. Rev. B **54**, 4320 (1996).
13. M.T. Béal-Monod, Phys. Rev. B **58**, 8830 (1998).
14. R. Nemetschek, R. Hackl, M. Opel, R. Philipp, M.T. Béal-Monod, J.B. Bieri, K. Maki, A. Erb, E. Walker, Eur. Phys. J. B **5**, 495 (1998).
15. B. Friedl, C. Thomsen, H.-U. Habermeier, M. Cardona, Solid State Commun. **78**, 291 (1991).
16. O.V. Misochko, E.Ya. Sherman, N. Umesaki, K. Sakai, S. Nakashima, Phys. Rev. B **59**, 11495 (1999).
17. I.I. Mazin, in *High Temperature Superconductivity*, edited by S.E. Barnes *et al.* (Woodbury, 1999), p. 79.
18. K. Takenaka, Y. Imanaka, K. Tamasaku, T. Ito, S. Uchida, Phys. Rev. B **46**, 5833 (1992).
19. R. Li, E.Ya. Sherman, R. Feile, G. Jakob, Th. Hahn, H. Adrian, Phys. Rev. B **53**, 6836 (1996).
20. R.F. Wood, M.A. Abdel-Raouf, Phys. Rev. B **51**, 11773 (1995).
21. R. Li, E.Ya. Sherman, R. Feile, G. Jakob, Th. Hahn, H. Adrian, Physica C **242**, 46 (1995).
22. D.L. Mills, A.A. Maradudin, E. Burstein, Ann. Phys. **56**, 504 (1970).
23. R. Loudon, Proc. Roy. Soc. A **275**, 218 (1963).
24. O.K. Andersen, O. Jepsen, A.I. Liechenstein, I.I. Mazin, Phys. Rev. B **49**, 4145 (1994).
25. Properties of two-dimensional systems demonstrating the Van Hove singularity were reviewed in R. Markiewicz, J. Phys. Chem. Solids **58**, 1179 (1997). However, we should take into account that a Van Hove singularity usually occurs in one-dimensional electronic systems as well. This fact implies that N_c can be of the same order of magnitude as N_p.
26. T.P. Devereaux, A. Virosztek, A. Zawadowski, Phys. Rev. B **51**, 505 (1995).
27. I.P. Ipatova, A.V. Subashiev, V.A. Schukin, Sov. Phys. Solid State **24**, 1932 (1982).